PHYSICAL REVIEW D **93,** 074508 (2016)

Dyons near the transition temperature in lattice QCD

V. G. Bornyakov
Institute for High Energy Physics NRC "Kurchatov Institute", 142281 Protvino, Russia,
Institute of Theoretical and Experimental Physics, 117259 Moscow, Russia,
and School of Biomedicine, Far East Federal University, 690950 Vladivostok, Russia

E.-M. Ilgenfritz
Joint Institute for Nuclear Research, BLTP, 141980 Dubna, Russia

B. V. Martemyanov
Institute of Theoretical and Experimental Physics, 117259 Moscow, Russia,
National Research Nuclear University MEPhI, 115409 Moscow, Russia,
and Moscow Institute of Physics and Technology, 141700 Dolgoprudny, Moscow Region, Russia

M. Müller-Preussker*
Institut für Physik, Humboldt-Universität zu Berlin, 12489 Berlin, Germany
(Received 8 February 2016; published 18 April 2016)

We study the topological structure of QCD by cluster analysis. The fermionic topological charge density is constructed from low-lying modes of the overlap Dirac operator for three types of temporal boundary conditions for the fermion field. This provides the possibility of marking all three dyon constituents of Kraan–van Baal–Lee–Lu (KvBLL) calorons in the gluonic fields. The gluonic topological charge density appears in the overimproved gradient flow process stopped at the moment when it maximally matches the fermionic topological charge density. This corresponds to the smearing of gluonic fields up to the scale set by dyon size. The timelike Abelian monopoles and specific KvBLL pattern of the Polyakov line are correlated with topological clusters.

DOI: 10.1103/PhysRevD.93.074508

I. INTRODUCTION

Two basic properties of QCD are the confinement of quarks and gluons and the spontaneous breaking of chiral symmetry at low temperature and density. Both properties are believed to be intimately connected with each other and to originate from a certain complex structure of the QCD vacuum state, the simplest manifestations of which being condensates of gluon and quark fields. The field fluctuations contributing to these condensates are, however, space-time and scale dependent. One of the aims of lattice gauge theory is to reveal the corresponding structures. One school of thought claims that—at the infrared scale—the origin of both mechanisms can be traced back to semiclassical objects of QCD. These objects either disappear or change their properties at high temperature, where the quark-gluon plasma phase appears.

Today it is commonplace to say that the instanton mechanism is able to explain chiral symmetry breaking while it fails to provide a mechanism for confinement. Without further sophistication, this is certainly correct for the instanton gas or liquid. Constituent dyons of Kraan–van Baal–Lee–Lu (KvBLL) calorons [1–3], however, are as good as instantons for explaining chiral symmetry breaking. With their dyon "substructure," calorons give some room to reproduce certain features of confinement (Polyakov loop correlators, spatial string tension, and vortex and/or monopole percolation), which was the reason why people expected for decades that "instanton quarks" might solve the confinement problem. Moreover, when considered as a rarefied gas, either without interaction or with Coulomb-like interaction, dyons give confining behavior for spacelike Wilson loops and for correlators of Polyakov loops. The history of this idea dates from the 1970s and has continued to the recent past [4–8].

The modeling of dyon ensembles with interaction has recently received even more attraction [9–14]. It is therefore of some interest to search for dyons in thermal Monte Carlo configurations (representing lattice gauge fields at different temperatures) in order to assess the relevance of these models and in order to eventually observe dyons clustering into caloronlike quasiclassical configurations.

The caloron with nontrivial holonomy [1–3] has the remarkable property that the single-zero mode of the Dirac operator is able to localize on distinct constituent dyons [15,16], depending on the temporal boundary condition (BC) applied to the Dirac operator, if the latter possesses improved chiral properties.

*Deceased.

Inspired by the KvBLL solutions, for a subset of thermal lattice configurations of fixed total topological charge $Q = \pm 1$ (created below and above $T_{\rm dec}$), the change of the single-zero mode's localization with the change of BC was observed by Gattringer *et al.* [17,18] and was interpreted in the caloron picture, ignoring other topological features of these configurations. In the case of $SU(2)$ and $SU(3)$ lattice gauge theory, it has been seen that this property of mobility (and the changing degree of localization) is shared by a band of near-zero modes (NZMs) of the overlap Dirac operator [19–22]. Thus, not only the set of zero modes reflecting the total topological charge of the gluonic field, but also the band of low-lying modes of the overlap Dirac operator identified with different boundary conditions can be used as effective tools to detect distinct topological objects. This direct insight from Monte Carlo configurations of lattice gauge fields (without cooling or smearing) is restricted, however, to a corresponding scale set by the eigenvalues. In the present paper we will see to what extent this technique leads us to the three dyons making up one "instanton" (caloron) of QCD.

In Sec. II we introduce the lattice setup in which the ensembles of gauge fields which we are going to analyze have been generated in lattice QCD with $N_f = 2$ dynamical flavors. In Sec. III we define all the topologically relevant lattice observables employed later on for the analysis. Then, in Sec. IV, the concrete case of $N_f = 2$ lattice QCD is considered at two temperatures, at the crossover T_χ (ensemble I) and at $T = 1.06T_\chi$ (ensemble II). The fermionic topological charge density was constructed with the help of low-lying modes of the overlap Dirac operator computed for three types of temporal boundary conditions.

We now introduce two ideas that are new compared to previous papers dealing with $SU(3)$ gluodynamics: (i) Again, in addition to antiperiodic boundary conditions for the overlap fermions, two other boundary conditions are employed in order to construct topological densities for each type of boundary condition. Here, however, the number of pairs of nonzero modes is not fixed for all boundary conditions; it is the eigenvalue cutoff that is fixed. We consider two cutoffs at two temperatures. An eigenvalue cutoff for nonzero modes of the Dirac operator, rather than a fixed number of modes (as was done earlier), is used in order to hide the ultraviolet fluctuations of the gluonic background. The eigenvalue cutoff is more directly related to the task of separating scales than the number of modes would be, in particular when different temperatures are considered. (ii) In order to characterize the configurations by the gluonic topological charge density, the technique of gradient flow has replaced the previously used cooling procedure. The gradient flow, a continuous cooling algorithm, is the most contemporary answer to the question of how to control the cooling; it introduces a scale parameter of the diffusion length. With hindsight, one could decide to cool up to the moment when diffusion length is of the order of the size of topological objects we are looking for, i.e., dyons. This is the reason to use the gradient flow, in which the scale parameter replaces the number of cooling steps. The stopping criterion is then set by the maximal approximation of the fermionic topological charge density by the gluonic one; thus, the gluonic topological density depends on the chosen cutoff scale. In this way, it will turn out that all UV fluctuations are removed, up to the size of dyons that we are searching for.

Finally, the properties of the clusters of the three fermionic topological densities under consideration are studied, including their correlations among each other as well as to the local holonomy and to the Abelian monopoles from the maximally Abelian gauge construction. In Sec. V we shall draw our conclusions.

II. LATTICE SETTING FOR THE THERMAL ENSEMBLES

We continue our study of topological objects in $SU(3)$ gauge theory in the case of QCD (with dynamical quarks). We have analyzed gauge-field configurations generated with the Wilson gauge action S_W and $N_f = 2$ dynamical flavors of nonperturbatively $O(a)$ improved Wilson fermions (clover fermions). These configurations were produced by the DIK Collaboration [23,24] using the Berlin QCD code [25]. The improvement coefficient c_{SW} was determined nonperturbatively [26]. The lattice spacing and pion mass were determined by the interpolation of $T = 0$ results obtained by the QCDSF Collaboration [27]. We have analyzed configurations produced on lattices with the temporal extent $L_\tau = 8$ and spatial sizes $L_s = 16$ (ensemble I of 50 configurations at $T = T_\chi$) and $L_\tau = 8$ and $L_s = 24$ (ensemble II of 50 configurations at $T = 1.06T_\chi$). The DIK Collaboration scanned the temperature T at fixed values of β by changing the Wilson fermion hopping parameter κ. In other words, the quark mass was not kept constant. The chiral crossover temperature $T_\chi \approx 230$ MeV was determined in Refs. [23,24] at a corresponding pion mass value of $O(1\ \text{GeV})$.

In Ref. [28] we investigated the T dependence of the topological susceptibility throughout the interval $[0.85T_\chi, 1.26T_\chi]$ by overimproved cooling applied to ensembles of 500 or 200 configurations, and we confronted the T dependence with the case of pure $SU(3)$ Yang-Mills theory (with Wilson action).

For the two temperatures $T = T_\chi$ and $T = 1.06T_\chi$, which we intend to investigate here with overlap fermions, with respect to details of the space-time topological structure (though for a smaller subensemble of 50 configurations each), we recall the topological susceptibility we found in Ref. [28]:

(i) ensemble I (500 configurations, overimproved cooling), $\chi_{\rm top} = (0.6 \pm 0.05)T_\chi^4$;
(ii) ensemble II (200 configurations, overimproved cooling), $\chi_{\rm top} = (0.3 \pm 0.03)T_\chi^4$.

III. TOPOLOGICALLY RELEVANT OBSERVABLES

In our analysis, we use the following instruments (observables):

(i) local holonomy and its trace (the Polyakov loop),
(ii) improved gluonic topological charge, and
(iii) Abelian monopoles revealed by Abelian projection after transforming the gauge field to the maximal Abelian gauge (MAG).

All these quantities are computed after gradient flow (in close correspondence to overimproved cooling). We also use the fermionic topological charge density (and its UV-filtered version), including its dependence on the temporal boundary conditions imposed on overlap fermions.

The importance and usefulness of the finite-temperature holonomy (considered globally to distinguish the phases of the theory and locally to distinguish the dyonic constituents or "instanton quarks") for the study of the topological structure was recognized only through the discovery of the KvBLL caloron solutions [1–3].

A. Holonomy

The local holonomy is defined as a product of timelike links

$$P(\vec{x}) = \prod_{x_0=1}^{N_\tau} U_0(\vec{x}, x_0). \tag{1}$$

$P(\vec{x})$ has eigenvalues

$$\lambda_k(\vec{x}) = \exp\left(i2\pi\mu_k(\vec{x})\right). \tag{2}$$

The positions in space of the dyon constituents of KvBLL calorons are determined by the condition that two of these eigenvalues coincide (cf. Appendix in [21]). We use this property to localize (anti)dyons in unsmoothed lattice field configurations.

The asymptotic holonomy of KvBLL calorons (after a suitable constant gauge transformation),

$$\mathcal{P}_\infty \equiv \lim_{|\vec{x}|\to\infty} P(\vec{x}) = \exp[2\pi i \mathrm{diag}(\mu_1, \mu_2, \mu_3)], \tag{3}$$

is characterized by the eigenphases, three real and ordered numbers $\mu_1 \le \ldots \le \mu_3 \le \mu_4 \equiv 1 + \mu_1$ fulfilling $\mu_1 + \mu_2 + \mu_3 = 0$. The set of eigenphases eventually determines the masses of well-separated dyon constituents via $8\pi^2\nu_m$, where $\nu_m \equiv \mu_{m+1} - \mu_m$ (cf. Appendix in [21]).

The trace of $P(\vec{x})$ is the gauge-invariant complex-valued Polyakov loop

$$L(\vec{x}) = \frac{1}{3}\mathrm{Tr}P(\vec{x}). \tag{4}$$

Its value can be represented as a point in the Weyl plot in the complex plane, see Fig. 6 in Sec. IV.

For $SU(3)$, when two eigenvalues of the local holonomy are equal, the respective Polyakov loop is represented by a point at the periphery of the Weyl plot. If all three eigenvalues coincide, the holonomy is an element of the center group

$$P(\vec{x}) = z_i \cdot I, \tag{5}$$

where

$$z_i \in \{1, \exp(2\pi i/3), \exp(-2\pi i/3)\}.$$

The expectation value of the spatially averaged Polyakov loop (V_3 is the spatial volume),

$$\bar{L} = \frac{1}{V_3}\sum_{\vec{x}} L(\vec{x}), \tag{6}$$

is an order parameter of the deconfinement transition in pure Yang-Mills gauge theory, signaling the breaking of the center symmetry. In the presence of dynamical fermions, this symmetry is—at best—only approximate, even at low temperature.

B. MAG and Abelian monopole definitions

We use the definition of the MAG introduced for lattice $SU(N)$ theory in [29] and later specified for the $SU(3)$ group in [30]. The MAG is fixed by maximizing the functional

$$F[U] = \frac{1}{12V}\sum_{x,\mu}[|(U_\mu(x))_{11}|^2 + |(U_\mu(x))_{22}|^2 + |(U_\mu(x))_{33}|^2] \tag{7}$$

with respect to local gauge transformations g of the lattice gauge field,

$$U_\mu(x) \to U^g_\mu(x) = g(x)^\dagger U_\mu(x) g(x+\hat{\mu}). \tag{8}$$

Alternative definitions of the MAG condition for the $SU(3)$ group were introduced in [31] and were studied further in [32]. To maximize the functional equation (7), we use the simulated annealing algorithm, which was found to be very effective in fighting the problem of Gribov copies [33]. It was first used in [34] for the $SU(3)$ gauge group; see also [35] for details of its implementation to the case of the $SU(3)$ gauge group. After fixing to the MAG, the Abelian fields $u_\mu(x) \in U(1) \times U(1)$ are determined as a result of the Abelian projection described in [29].

The monopole currents $j^{(a)}_\mu(^*x)$ are defined [29] on links of the dual lattice and satisfy the current conservation law for every a separately,

$$\sum_{\mu} \partial_{\mu}^{-} j_{\mu}^{(a)}(^{*}x) = 0, \quad a = 1, 2, 3. \tag{9}$$

Additionally,

$$\sum_{a=1}^{3} j_{\mu}^{(a)}(^{*}x) = 0; \tag{10}$$

i.e., only two currents are independent.

C. The gluonic definition of the topological density

The definition of topological charge density is

$$q(x) = \frac{1}{16\pi^2} \mathrm{Tr}(F_{\mu\nu}(x)\tilde{F}_{\mu\nu}(x)), \tag{11}$$

where

$$\tilde{F}_{\mu\nu}(x) = \frac{1}{2}\epsilon_{\mu\nu\lambda\sigma}F_{\lambda\sigma}(x). \tag{12}$$

The lattice gluonic topological charge density uses the field strength definition of $F_{\mu\nu}(x)$ as a "clover" average over the traceless anti-Hermitian part of all four plaquettes within the $\mu\nu$ plane, with side length $n = 1$ placed around a site x while kept untraced in that site x. The improved topological charge density [36] extends this construction to quadratic loops of sizes $n = 2$, 3, which are added with appropriate weights. The improved topological charge and corresponding action (in units of the one-instanton action S_{inst}) are then defined as

$$Q_{\mathrm{glue}} = \sum_{x} \mathrm{Tr}(F_{\mu\nu}(x)\tilde{F}_{\mu\nu}(x))/(16\pi^2), \tag{13}$$

$$S/S_{\mathrm{inst}} = \sum_{x} \mathrm{Tr}(F_{\mu\nu}(x)F_{\mu\nu}(x))/(16\pi^2). \tag{14}$$

D. Overimproved gradient flow

Gradient flow is an advanced method to remove quantum fluctuations up to a certain "diffusion" scale from given lattice field configurations created in the course of Monte Carlo simulations [37]. The gradient flow effectively also results in a minimization of the action in the "direction" of the steepest descent in configuration space [38–40]. Proposed by Lüscher for the Wilson (one-plaquette) action, the gradient flow can be defined with respect to different gluonic actions, of which the Wilson flow realizes the simplest case. In our case, we propose to use the gradient flow with respect of an action of the form

$$S(\epsilon) = \sum_{x,\mu\nu} \frac{4-\epsilon}{3} \mathrm{Re\ Tr}(1 - U_{x,\mu\nu}) + \sum_{x,\mu\nu} \frac{\epsilon - 1}{48} \mathrm{Re\ Tr}(1 - U^{2\times 2}_{x,\mu\nu}), \tag{15}$$

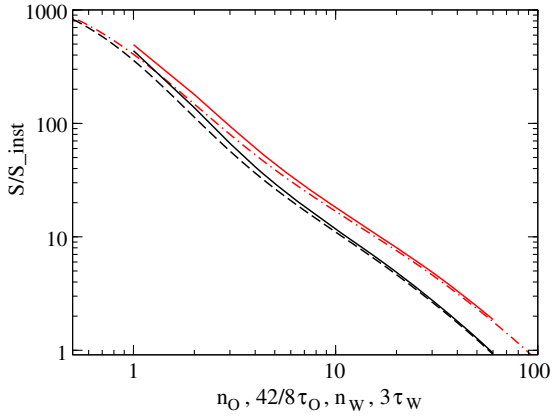

FIG. 1. The evolution of action (14) (in instanton units) with the Wilson cooling step n_W (black line) and with Wilson flow time $3\tau_W$ (black dashed line) shown on the abscissa, and the variation of the same action (14) (in the same units) with the overimproved cooling step n_O (red line) and with overimproved flow time $(42/8)\tau_O$ shown on the abscissa (red dash-dotted line).

which reduces to the Wilson action in the case $\epsilon = 1$. The so-called overimproved action [41] corresponds to $\epsilon = -1$. Expanding in powers of lattice spacing a, one finds that the lattice action now includes higher-dimension operators,

$$S(\epsilon) = \sum_{x,\mu\nu} a^4 \mathrm{Tr}\left[\frac{1}{2}F^2_{\mu\nu}(x) - \frac{\epsilon a^2}{12}(D_\mu F_{\mu\nu}(x))^2\right] + O(a^8). \tag{16}$$

For a discretized continuum instanton of size ρ this provides corrections of order a/ρ,

$$S(\epsilon) = 8\pi^2\left[1 - \frac{\epsilon}{5}\left(\frac{a}{\rho}\right)^2 + \mathcal{O}\left(\left[\frac{a}{\rho}\right]^4\right)\right], \tag{17}$$

suggesting that undercooling ρ will decrease for $\epsilon > 0$ and increase for $\epsilon < 0$. The inversion of lattice artefacts relative to the Wilson case makes topological lumps stable against the process of gradient flow.

It is worth noting that standard gradient flow or Wilson flow [38–40] ($\epsilon = 1$) can be mapped one to one [42] to standard Wilson cooling. It is seen from Fig. 1 that the same holds for over-improved gradient flow in the sense that it nicely follows over-improved cooling.

E. UV filtered fermionic topological charge density

We consider the NZM band of eigenmodes of the massless overlap operator D. We use the overlap Dirac operator D of the form [43,44]

$$D(m=0) = \frac{\rho}{a}\left(1 + \frac{D_W}{\sqrt{D_W^\dagger D_W}}\right) = \frac{\rho}{a}(1 + \mathrm{sgn}(D_W)), \tag{18}$$

where $D_W = M - \rho/a$, M is the hopping term of the Wilson-Dirac operator and ρ/a is a negative mass term usually determined by optimization. The index of D can be identified with the integer-valued topological charge $Q_{\rm over}$ [45]. The nonzero modes have vanishing chirality and appear in pairs, with modes in the pair related by $\psi_\lambda = \gamma_5 \psi_{-\lambda}$.

For the configurations with $L_\tau = 8$ and spatial size $L_s = 16$ at $T = T_\chi$ (ensemble I with 50 configurations), we found from the average square of the number of zero modes (equal to $\langle Q^2 \rangle$) $\chi_{\rm top} = (0.71 \pm 0.17) T_\chi^4$. For ensemble II with 50 configurations, with $L_\tau = 8$ and spatial size $L_s = 24$ at $T = 1.06 T_\chi$, we found $\chi_{\rm top} = (0.24 \pm 0.05) T_\chi^4$. The comparison of these numbers with those of overimproved cooling reported in Sec. II (the agreement is within 4% or 6% for the fourth root of the susceptibility) specifies the systematical error induced by the cooling method.

The fermionic topological charge density with maximal resolution (down to the lattice spacing a) is defined in terms of the overlap Dirac operator (18) as follows:

$$q(x) = -\mathrm{tr}\left[\gamma_5 \left(1 - \frac{a}{2\rho} D(m=0;x,x)\right)\right]. \quad (19)$$

Using the spectral representation of (19) after diagonalization in terms of the eigenmodes $\psi_\lambda(x)$, a UV-filtered form of the density can be defined as a sum over narrow band of NZMs,

$$q_{\lambda_{\rm sm}}(x) = -\sum_{|\lambda|<\lambda_{\rm sm}} \left(1 - \frac{\lambda}{2}\right) \sum_c (\psi_\lambda^c(x), \gamma_5 \psi_\lambda^c(x)), \quad (20)$$

with $\lambda_{\rm sm}$ acting as a UV cutoff.

The diagonalization of the overlap operator is achieved using a variant of the Arnoldi algorithm [46]. We had at our disposal between 20 and 30 nonzero eigenmodes.

While the physical fermion sea is described by the Dirac operator implemented with antiperiodic temporal boundary conditions, for the purpose of analyzing the topological structure it is useful to diagonalize the Dirac operator subject to continuously modified temporal boundary conditions characterized by an angle ϕ,

$$\psi(\vec{x}, x_4 + \beta) = \exp(i\phi)\psi(\vec{x}, x_4). \quad (21)$$

The reason is that a caloron with nontrivial holonomy has the remarkable property that the single-zero mode of the Dirac operator is able to localize on distinct constituent dyons [15,16], depending on the temporal BC applied to the Dirac operator if the latter possesses improved chiral properties. In the case of $SU(2)$ and $SU(3)$ lattice gauge theory, it has been seen that this property of mobility (and changing degree of localization) is also shared by a band of near-zero modes of the overlap Dirac operator [19–22].

We have chosen three angles including the case of antiperiodic boundary condition,

$$\phi = \left\{ \begin{array}{l} \phi_1 \equiv -\pi/3 \\ \phi_2 \equiv +\pi/3 \\ \phi_3 \equiv \pi \end{array} \right\}, \quad (22)$$

thus ensuring for a single caloron solution that the corresponding fermion zero modes become maximally localized at one, but each time at a different one, of its three constituent dyons. Note that ϕ_3 corresponds to the antiperiodic boundary condition.

The construction of the UV-smoothed topological charge density in terms of the eigenvalues and eigenmodes should be specifically done for the three boundary conditions

$$q_{i,\lambda_{\rm sm}}(x) = -\sum_{|\lambda|<\lambda_{\rm sm}} \left(1 - \frac{\lambda}{2}\right) \sum_c (\psi_{i,\lambda}^c(x), \gamma_5 \psi_{i,\lambda}^c(x)), \quad (23)$$

where $i = 1, 2, 3$ enumerates the three boundary conditions defined by Eq. (22).

For the configurations with $L_\tau = 8$ and spatial sizes $L_s = 16$ (ensemble I with 50 configurations at $T = T_\chi$) we take $\lambda_{\rm sm} = 331$ MeV. This is the minimal spread of $|\lambda|$ among the 20 nonzero eigenvalues we have found per configuration (i.e., minimal with respect to all 50 configurations and 3 boundary conditions). For the configurations with $L_\tau = 8$ and spatial sizes $L_s = 24$ (ensemble II with 50 configurations at $T = 1.06 T_\chi$) we take $\lambda_{\rm sm} = 254$ MeV; this is the minimal spread of $|\lambda|$ among 30 eigenvalues per configuration, which we have determined by diagonalization. The actual number of nonzero modes falling into this interval and being included in the definition Eq. (20) fluctuates from configuration to configuration because in the present analysis an eigenvalue cutoff is applied instead of a fixed number of modes.

We remark that in the case of ensemble I we have also considered, aside from the cutoff $\lambda_{\rm sm} = 331$ MeV, the smaller cutoff $\lambda_{\rm sm} = 254$ MeV known from ensemble II. This implies that the construction of the topological density includes fewer nonzero modes than for the larger cutoff. This will allow us to discuss the effect of changing the cutoff for ensemble I (representing the lower temperature) and to compare the two temperatures (applying the smaller cutoff both to ensemble I and ensemble II).

The localization of the topological charge within a given charge density filling a lattice configuration can be measured by the inverse participation ratio (IPR), which ranges between the extremes of 1 (totally delocalized) and V_4 (fully localized). It is defined as

$$\mathrm{IPR} = V_4 \frac{\sum_x |q(x)|^2}{(\sum_x |q(x)|)^2}, \quad (24)$$

TABLE I. Inverse participation ratio (IPR) of the fermionic topological charge density at the selected fermionic cutoff $\lambda_{\rm sm}$, for three types of boundary conditions.

Type of boundary condition	Ensemble I $\lambda_{\rm sm} = 331$ MeV	Ensemble I $\lambda_{\rm sm} = 254$ MeV	Ensemble II $\lambda_{\rm sm} = 254$ MeV
First type BC	2.279(30)	2.373(36)	3.312(76)
Second type BC	2.282(29)	2.428(36)	3.259(84)
Third type BC	2.354(35)	2.493(45)	8.436(964)

where V_4 is the four dimensional volume. Any subvolume fV_4 that is equally filled results in IPR $= 1/f$. Using Eq. (24), we have analyzed the IPR of the three types of fermionic toplogical charge density corresponding to the three boundary conditions, at both temperatures for the same cutoff, and for the lower temperature (at T_χ) with two different cutoffs. The result is presented in Table I.

We can conclude that at the equal cutoff $\lambda_{\rm sm} = 254$ MeV for antiperiodic boundary conditions, the localization is three times bigger at the higher temperature $T = 1.06T_\chi$ compared to $T = T_\chi$. In addition, at the higher temperature, antiperiodic boundary conditions result in a localization by a factor of 2.5 stronger than the other two boundary conditions.

At the lower temperature T_χ, the lower cutoff $\lambda_{\rm sm} =$ 254 MeV leads only to a few-percent increase of localization as compared to the larger cutoff $\lambda_{\rm sm} = 331$ MeV. The effect of changing boundary conditions is at a similar level.

We will compare the fermionic topological density $q_f(x)$, truncated according to (23) with a fixed cutoff $\lambda_{\rm sm}$ and averaged over the boundary conditions, with the gluonic topological density $q_g(x)$ (11), provided that a suitable amount of overimproved gradient flow has been applied to the gauge-field configuration. Before we can make the comparison, both topological densities should be corrected (by a shift [47]) to have a vanishing volume average,

$$q_g(x) \to q_g(x) - \bar{q}_g \tag{25}$$

and

$$q_f(x) \to q_f(x) - \bar{q}_f. \tag{26}$$

The optimal matching between the two (corrected) topological densities is achieved when the properly normalized "scalar product" between the two topological densities $q_g(x) - \bar{q}_g$ and $q_f(x) - \bar{q}_f$, expressed by the cosine between "direction vectors,"

$$\cos(\theta) = \frac{\sum_x (q_g(x) - \bar{q}_g) \cdot (q_f(x) - \bar{q}_f)}{\sqrt{\sum_x (q_g(x) - \bar{q}_g)^2 \cdot \sum_x (q_f(x) - \bar{q}_f)^2}}, \tag{27}$$

passes a maximum. Figure 2 shows the rise of the cosine towards the maximum for the 50 individual configurations of both ensembles, ensemble I (left panel) and ensemble II (right panel), as function of the flow time τ_O, until the flow is stopped at the maximum of the cosine.

Figure 3 shows the step number (corresponding to the adoption of a finite-flow time step $\Delta\tau = 0.02$ adopted) linearly growing until the overimproved gradient flow is stopped. This necessary step number fluctuates from configuration to configuration. Let us note that the average step number ($\approx$100) of the overimproved gradient flow corresponds to a flow time $\tau_O \approx 2$. This is the time required to let the diffusion length [48] of gradient flow, $\sqrt{8\tau_O}$, grow

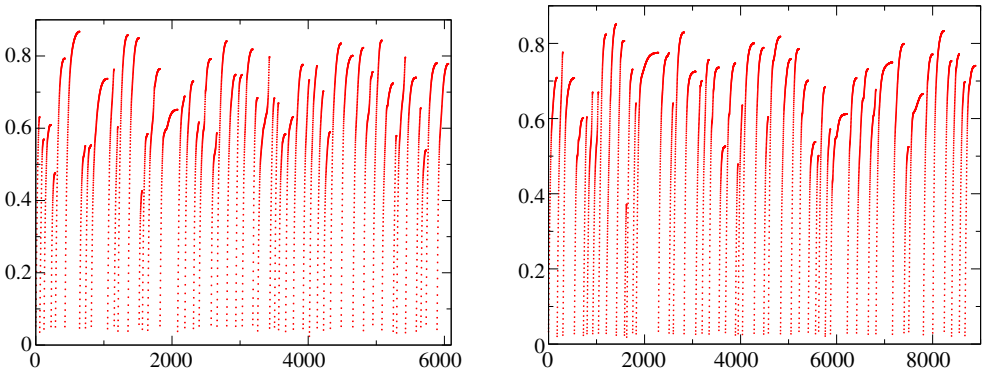

FIG. 2. The evolution of the cosine $\cos(\theta)$, the cosine of an "angle" between gluonic and fermionic topological charge density (see text), shown as function of common flow time ($\tau_O/\Delta\tau$), consecutively for all 50 configurations of ensemble I (left panel) and ensemble II (right panel).

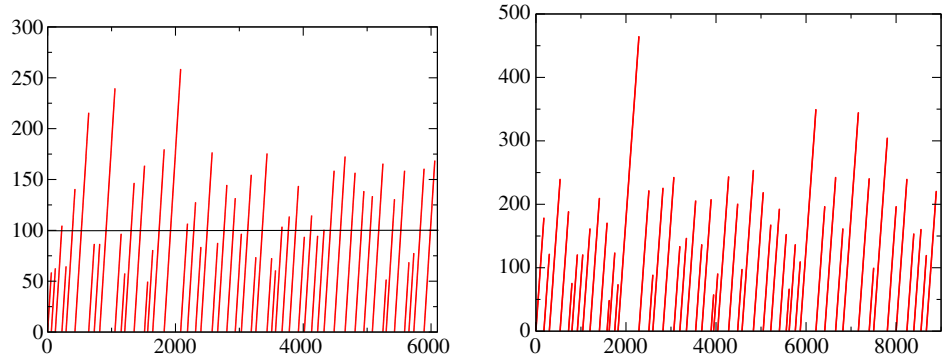

FIG. 3. The number of steps of overimproved gradient flow ($\tau_O/\Delta\tau$) (with step size $\Delta\tau = 0.02$) growing until the cosine reaches the maximum; i.e., the best matching is achieved between the gluonic topological charge density and the fermionic topological charge density (averaged over boundary conditions). All 50 configurations of ensemble I (left panel) and ensemble II (right panel) are shown.

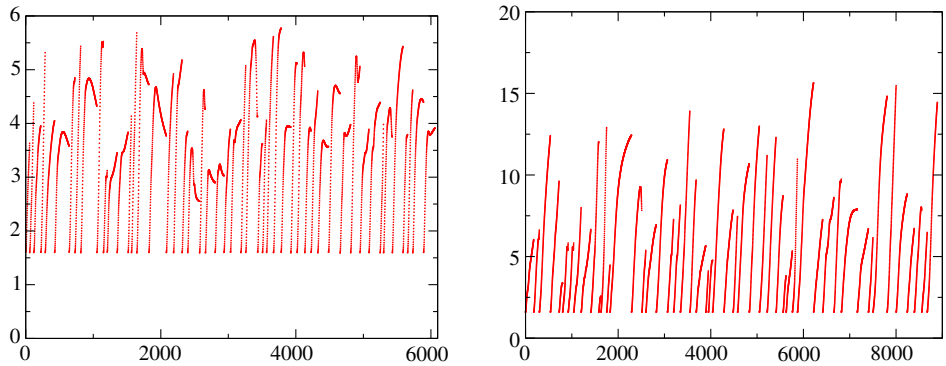

FIG. 4. The IPR of the gluonic topological charge density evolving in the course of overimproved gradient flow ($\tau_O/\Delta\tau$) until the best matching between the gluonic topological charge density and the fermionic topological charge density (averaged over boundary conditions) is achieved. All 50 configurations of ensemble I (left panel) and ensemble II (right panel) are shown.

to the size of a dyon, $1/(2\pi\nu_d T)$ where $\nu_d = \nu_1 = \nu_2 = \nu_3 = 1/3$ [1–3]. This would adequately describe the fractional charges in the case of maximally nontrivial holonomy (i.e., a vanishing average Polyakov loop). This average step number is shown by a horizontal line in the left panel of Fig. 3, which represents the smoothing of ensemble I. The averaged value of dimensionless quantity $t_O^2 \cdot \frac{1}{2}\mathrm{Tr}(F_{\mu\nu}(x)F_{\mu\nu}(x))$ (with the dimensionful flow time $t_O = a^2\tau_O$) is equal to 0.37 in the case of ensemble I and 0.34 for ensemble II. This fits remarkably well to the generally used stopping criterion for Wilson flow [38–40].

Figure 4 shows for each configuration how the IPR of the gluonic topological density evolves in the course of gradient flow, until the average fermionic density is optimally matched. The filling fraction f changes from $1/3$ to $1/10$ with the increase of temperature (see also the IPR for the fermionic topological charge density).

Topologically nontrivial clusters filtered out with the three truncated fermionic densities (23), each corresponding to one type of fermionic boundary condition, will be separately considered in the following as topologically different objects (dyon candidates). Their localization was previously described by a corresponding IPR (see Table I). They may appear either as isolated or as forming compounds with other dyons (dyon-dyon pairs) or antidyons (dyon-antidyon pairs), including the possibility of recombining into calorons.

IV. RESULTS OF CLUSTER ANALYSIS FOR THE QCD ENSEMBLES

In the following we will analyze our two QCD ensembles of thermalized configurations along the lines sketched above. In order to identify topological clusters of the lattice gauge fields with the help of the low-lying spectrum of the overlap operator, we used a fixed cut on eigenvalues $\lambda_{\mathrm{sm}} = 331$ MeV for configurations with $L_s = 16$, $T = T_\chi$ (see above). For configurations with $L_s = 24$ (50 configurations at $T = 1.06T_\chi$) we take $\lambda_{\mathrm{sm}} = 254$ MeV. In all three sectors (selected by the angles ϕ_i) the fermionic topological density is constructed.

For the purpose of detecting gluonic features of (anti) dyon excitations among such clusters we have made the configurations undergo the procedure of overimproved gradient flow until the gluonic topological density profiles

optimally matched the fermionic one averaged over sectors, analogously to what we did in our previous paper [21] where we followed the concept of an equivalent filtering as developed in [47,49,50]. This filtering is in particular acting on (smoothing) the local holonomy, while the gluonic topological density fits, by construction, to the sector-averaged fermionic density.

We have first applied the same cluster analysis as in our previous paper [21] with a variable lower cutoff $q_{\rm cut} > 0$ in order to characterize the cluster properties of the three density functions Eq. (23) in the thermal ensembles.

Let us summarize here the idea of the cluster algorithm. In the first step, for each of the three fermionic boundary conditions [Eq. (22)], the algorithm identifies the lattice points forming the interior of *all* clusters (the so-called "topological cluster matter") defined by the condition $|q(x)| > q_{\rm cut}$. The crucial second step is to require the connectedness between the lattice points in order to form individual extended clusters out of this cluster matter. Neighboring points with $|q(x)|$ above the threshold and sharing the same sign as the topological charge density are declared to belong to the same cluster. The cutoff $q_{\rm cut}$ has been chosen such as to resolve the given "continuous" distribution $q(x)$ into a maximal number of internally connected and mutually separated clusters. The cutoff value has been independently adapted for each configuration.

For ensemble I, the difference between the two cutoff values $\lambda_{\rm sm}$ is small. Between the two levels of gradient flow, the resulting numbers of all clusters $N_{\rm cl}$ coincide within errors. On the other hand, the same cutoff $\lambda_{\rm sm} = 254$ MeV applied to lattices with different volumes $[V_4(II)/V_4(I) = (3/2)^3/(1.06)^4 \approx 2.67]$ provides us with the possibility to understand the size of finite volume effects: all extensive quantities (as it can be seen from Table I) differ from each other by a factor of order 2.

There are two conditions for checking the dyonic nature of isolated clusters: (1) an integrated topological charge of close to $\pm$ one third and (2) the existence of a point inside of cluster where two eigenvalues of the local holonomy become degenerate.

If the holonomy is represented by the local Polyakov loop, this second condition corresponds to a position of that point in the clusters' Weyl plot close to one of its three sides. According to the type of fermionic boundary condition that is applied, one can anticipate which side of the Weyl plot should be approached: the left side corresponds to antiperiodic boundary conditions ϕ_3, the upper right side corresponds to ϕ_2, and the lower right side corresponds to ϕ_1. Among all points belonging to a cluster, we have searched for a minimum of the distance to the corresponding side of the Weyl plot. In this way we have defined which point should be considered as the "center of the cluster" (compare Fig. 6).

In order to find the integrated topological charge of the clusters, we use the gluonic topological charge density as it appears after applying the gradient flow process required to match the gluonic topological charge density to the fermionic one. In this case we find clusters of the gluonic topological charge density in the same way as we previously found clusters of fermionic topological charge density, according to three different types of fermionic boundary conditions.

If, for example, the extrema of the clusters of fermionic topological charge density for the first type of BC (with timelike monopole links inside) fall into a cluster of gluonic topological charge, we say that this gluonic topological cluster contains a dyon of the first type. The same procedure is applied to identify the character of other types of dyons. This gives us the possibility of sorting all gluonic topological clusters into the following categories: as full calorons (three different dyons inside), as three types of dyon pairs (two different dyons inside), as three types of dyons (one dyon inside), or as background (no dyons inside).

For isolated dyons and dyon pairs and for full calorons, we find the integrated topological charges the same way as we do for isolated dyons and calorons in the case of $SU(2)$ objects [51]. The results can be seen in Fig. 5 for ensemble II.

There is another question to be checked, i.e., the correlation of Abelian monopoles with the timelike currents in the Abelian projection after MAG. This is particularly interesting at much higher temperatures, where Abelian monopoles become thermal (cyclic) and almost static (exclusively timelike). Even close to the transition, like in our case, this might sharpen the test for clusters being actually dyons or antidyons.

All quantitative data on the correlations between the topological charge density and the MAG monopole content is presented in Table II.

Our main results on the correlation of low-lying modes of the overlap Dirac operator (as represented by the clusters of fermionic topological charge) with the Abelian

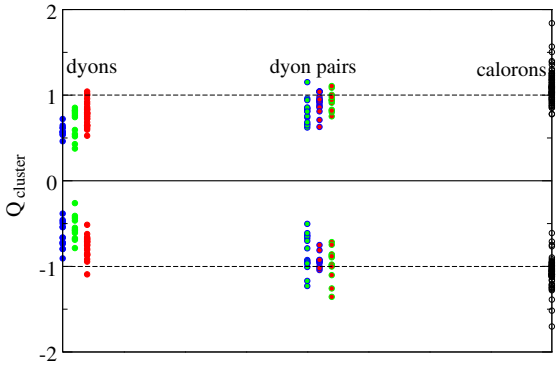

FIG. 5. The integrated topological charges of gluonic topological clusters interpreted as three types of dyons, as three types of dyon pairs, and as full calorons (analyzed for ensemble II). The color code refers to the type of dyon.

TABLE II. Results of the cluster analysis using low-lying overlap operator modes with three kinds of boundary conditions. All numbers indicate averages per configuration. The pure statistical errors are given in parentheses. We denote by $V_{\rm cl}$ the volume fraction occupied by all topological clusters; by $V_{\rm cl\ mon}$, the volume fraction occupied by clusters identified to contain time-like magnetic monopoles; by $N_{\rm cl}$, the number of all clusters per configuration; by $N_{\rm cl\ mon}$, the number of clusters identified to contain timelike magnetic monopoles; by $N_{\rm mon}$, the overall number of dual timelike links carrying monopole currents; by $N_{\rm mon\ cl}$, the number of dual timelike links carrying monopole currents found inside topological clusters; by $N_{\rm loop}$, the overall number of thermally closed monopole worldlines; and by $N_{\rm loop\ cl}$, the number of thermally closed monopole worldlines piercing topological clusters. The first part of the table is related to ensemble I ($L_s = 16$ at $T = T_\chi$). Here we show the effect of changing the cutoff from $\lambda_{\rm sm} = 331$ MeV (derived for 20 eigenmodes) to a smaller cutoff $\lambda_{\rm sm} = 254$ MeV (implying more iterations of gradient flow). The second part of the table is related to ensemble II ($L_s = 24$ at $T = 1.06T_\chi$), where the cutoff $\lambda_{\rm sm} = 254$ MeV (derived for 30 eigenmodes) has been applied.

Type of clusters	$V_{\rm cl}$	$V_{\rm cl\ mon}$	$N_{\rm cl}$	$N_{\rm cl\ mon}$	$N_{\rm mon}$	$N_{\rm mon\ cl}$	$N_{\rm loop}$	$N_{\rm loop\ cl}$
Clusters obtained with lowest overlap modes for $16^3 \times 8$ configurations								
First-type clusters	6.7(8)%	6.1(8)%	12.9(3)	3.5(2)	⋯	32(3)	⋯	5.4(4)
Second-type clusters	6.0(7)%	5.2(7)%	13.1(3)	3.7(2)	⋯	30(2)	⋯	5.4(4)
Third-type clusters	6.1(8)%	5.5(8)%	12.0(4)	3.6(2)	⋯	31(2)	⋯	5.1(4)
All clusters ($\lambda_{\rm sm} = 331$ MeV)	11(1)%	10(1)%	38(1)	10.8(6)	129(4)	45(3)	8.7(5)	6.4(4)
All clusters ($\lambda_{\rm sm} = 254$ MeV)	12(1)%	11(1)%	32(1)	9.6(6)	120(4)	42(3)	8.1(5)	5.8(4)

Type of clusters	$V_{\rm cl}$	$V_{\rm cl\ mon}$	$N_{\rm cl}$	$N_{\rm cl\ mon}$	$N_{\rm mon}$	$N_{\rm mon\ cl}$	$N_{\rm loop}$	$N_{\rm loop\ cl}$
Clusters obtained with lowest overlap modes for $24^3 \times 8$ configurations								
First-type clusters	5.1(3)%	4.4(4)%	24(1)	5.8(3)	⋯	59(3)	⋯	9.9(6)
Second-type clusters	6.2(6)%	5.5(6)%	24(1)	5.5(3)	⋯	64(4)	⋯	10.6(7)
Third-type clusters	1.8(2)%	1.5(2)%	11(1)	5.7(4)	⋯	40(3)	⋯	6.7(6)
All clusters ($\lambda_{\rm sm} = 254$ MeV)	8.0(6)%	7.0(6)%	59(2)	17.0(8)	193(8)	76(5)	20.2(8)	12.1(7)

monopoles of MAG are as follows. For ensemble I (ensemble II) the topological clusters occupy about 11% (8%) of the lattice 4-volume, whereas topological clusters constrained to contain static MAG monopole currents cover 10% (7%) of the lattice volume; the latter, however, contain about 35% (40%) of the timelike dual links carrying MAG monopoles. Inside those topological clusters, which are pierced by MAG monopoles, the density of monopoles is about 5 (9) times larger than it is outside these clusters. These numbers become even more pronounced if one counts not just the timelike monopole currents (dual links) in topological clusters but also the numbers of thermal monopoles piercing topological clusters. Around 75% (60%) of thermal (thermally winding) monopoles are seen to be piercing topological clusters.

We expect that the topological clusters detected with antiperiodic boundary conditions (in our case with a real-valued average Polyakov loop) can be viewed as related to more-heavy dyons: at the higher temperature $T = 1.06T_\chi$ (in ensemble II), they are expected to become statistically suppressed because of their higher action in comparison with the other constituents of a caloron. The number of clusters of the third type in ensemble II (see the lower part of Table II) is more than two times lower than the numbers of clusters of the first and second types. We can further estimate the suppression quantitatively by measuring the abundance of thermal monopoles piercing topological clusters of the third type compared to those piercing topological clusters of the first or second type. We are inclined to associate such thermal monopoles, if they are correlated with clusters of topological charge, with physical dyons. We found the proportion 9.9∶10.6∶6.7 (see the lower part of Table II). Thus, the heavier caloron constituent clusters are suppressed even when the temperature exceeds T_χ by only few percent.

Furthermore, the correlation between the local Polyakov loop on one side and the dyon nature of clusters of topological charge on the other is increased if the clusters are constrained to coincide with Abelian monopoles. The Polyakov loop tests the degeneracy of holonomy eigenvalues in the cluster centers that are, by our definition above, distinguished among all the cluster points by the condition of having a minimal distance from the sides of the Weyl plot.

We show in the lower panels of Fig. 6 scatter plots of local Polyakov loops measured in the centers of the clusters that are associated with magnetic monopoles. Since the clusters are labeled by one of the three boundary conditions for the fermionic modes (used to define the fermionic topological charge density), the scatter plot on the Weyl plot, Fig. 6, shows the different regions of population. The tendency of the Polyakov loop in the cluster centers to concentrate along the corresponding sides of the Weyl plot is much more pronounced than it was for all clusters (Fig. 6, upper panels). We recall that the Polyakov loop is measured for the gluonic field that has emerged from the gradient flow at the maximal matching of gluonic and fermionic topological densities.

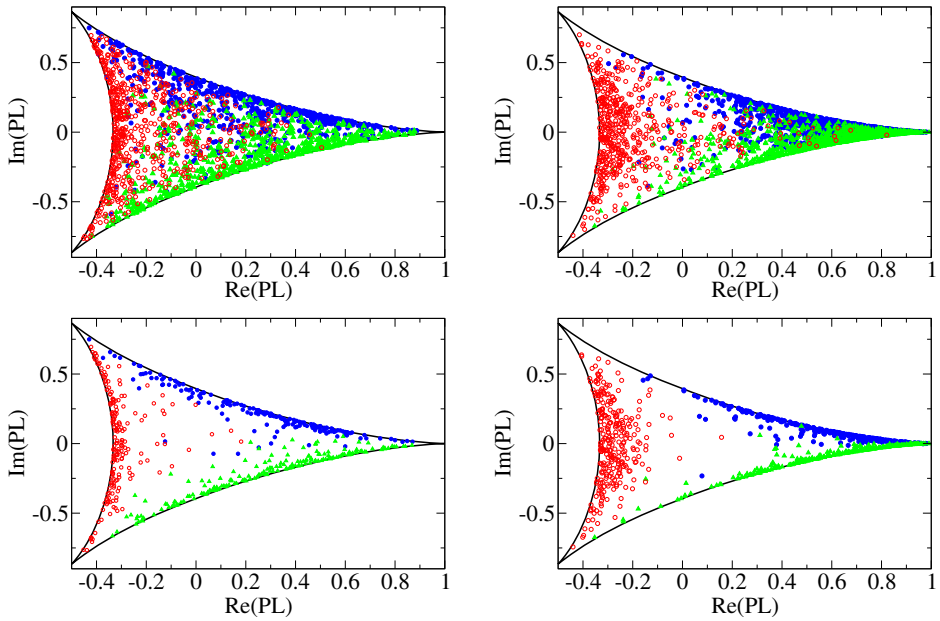

FIG. 6. Scatter plots of Polyakov loops (PLs) for configurations that have undergone the overimproved gradient flow procedure in the centers of all clusters (upper row) and of clusters selected to contain monopoles (lower row). The clusters are separated according to the type of boundary condition for the overlap near-zero modes. For clusters of the first type, the Polyakov loop is shown by green triangles; for clusters of second type, by blue filled circles; and for clusters of third type, by red open circles. The scatter plots show all clusters of all 50 configurations of size $L_s = 16$ and $T = T_\chi$ on the left (ensemble I) and size $L_s = 24$ and $T = 1.06T_\chi$) on the right (ensemble II).

V. CONCLUSIONS

We have discussed, for lattice QCD, the dyonic signatures of clusters of topological charge selected by using three types of temporal boundary conditions that were applied to the overlap modes used in the fermionic definition of topological density. In contrast to our previous paper on $SU(3)$ gluodynamics [22], for the construction of fermionic topological densities here, it is not the number of pairs of near-zero modes is fixed but instead the eigenvalue cutoff. The thermal lattice gauge fields were generated close to the crossover temperature. Topological clusters considered as candidates to be dyons were established by filtering, i.e., restricting ourselves to low-lying modes of the overlap Dirac operator with specific boundary conditions. Additionally, we have applied the procedure of overimproved gradient flow (instead of overimproved cooling, which was used in [22]) to the gluonic lattice fields, after which a similar pattern of clusters occurs within the gluonic topological charge distribution (which is, however, averaged over boundary conditions). We looked for distributions of the local Polyakov loop and searched for MAG monopole currents in the gradient-flow-smeared gluonic fields. We found clear correlations of the topological clusters with thermal monopoles as well as with lattice sites, where the local holonomy has close-to-degenerate eigenvalues. All this points to the correctness of an interpretation of clusters in terms of (anti)dyon excitations of the KvBLL type, and it has enabled us to estimate corresponding densities and cluster properties.

ACKNOWLEDGMENTS

B. V. M. appreciates the support of Humboldt University of Berlin, where the main part of the work was done. He also has been supported by Grants No. RFBR 13-02-01387a and No. 15-02-07596a. E.-M. I. and M.M.-P. acknowledge financial support by the Heisenberg-Landau Program between the German BMBF and BLTP of JINR Dubna.

[1] T. C. Kraan and P. van Baal, Nucl. Phys. **B533**, 627 (1998).
[2] T. C. Kraan and P. van Baal, Phys. Lett. B **435**, 389 (1998).
[3] K. Lee and C. Lu, Phys. Rev. D **58**, 025011 (1998).
[4] A. M. Polyakov, Nucl. Phys. **B120**, 429 (1977).
[5] B. V. Martem'yanov and S. V. Molodtsov, JETP Lett. **65**, 142 (1997).
[6] P. Gerhold, E.-M. Ilgenfritz, and M. Müller-Preussker, Nucl. Phys. **B760**, 1 (2007).

[7] D. Diakonov and V. Petrov, Phys. Rev. D **76**, 056001 (2007).
[8] F. Bruckmann, S. Dinter, E.-M. Ilgenfritz, B. Maier, M. Müller-Preussker, and M. Wagner, Phys. Rev. D **85**, 034502 (2012).
[9] E. Shuryak, J. Phys. G **39**, 054001 (2012).
[10] P. Faccioli and E. Shuryak, Phys. Rev. D **87**, 074009 (2013).
[11] R. Larsen and E. Shuryak, arXiv:1408.6563.
[12] Y. Liu, E. Shuryak, and I. Zahed, Phys. Rev. D **92**, 085006 (2015).
[13] Y. Liu, E. Shuryak, and I. Zahed, Phys. Rev. D **92**, 085007 (2015).
[14] R. Larsen and E. Shuryak, Phys. Rev. D **92**, 094022 (2015).
[15] M. García Pérez, A. González-Arroyo, C. Pena, and P. van Baal, Phys. Rev. D **60**, 031901 (1999).
[16] M. N. Chernodub, T. C. Kraan, and P. van Baal, Nucl. Phys. B, Proc. Suppl. **83–84**, 556 (2000).
[17] C. Gattringer, Phys. Rev. D **67**, 034507 (2003).
[18] C. Gattringer and S. Schaefer, Nucl. Phys. **B654**, 30 (2003).
[19] V. G. Bornyakov, E.-M. Ilgenfritz, B. V. Martemyanov, S. M. Morozov, M. Müller-Preussker, and A. I. Veselov, Phys. Rev. D **76**, 054505 (2007).
[20] V. G. Bornyakov, E.-M. Ilgenfritz, B. V. Martemyanov, and M. Müller-Preussker, Phys. Rev. D **79**, 034506 (2009).
[21] E.-M. Ilgenfritz, B. V. Martemyanov, and M. Müller-Preussker, Phys. Rev. D **89**, 054503 (2014).
[22] V. G. Bornyakov, E. M. Ilgenfritz, B. V. Martemyanov, and M. Muller-Preussker, Phys. Rev. D **91**, 074505 (2015).
[23] V. G. Bornyakov *et al.* (DIK Collaboration), Phys. Rev. D **71**, 114504 (2005).
[24] V. G. Bornyakov, R. Horsley, S. M. Morozov, Y. Nakamura, M. I. Polikarpov, P. E. L. Rakow, G. Schierholz, and T. Suzuki (QCDSF-DIK Collaboration), Phys. Rev. D **82**, 014504 (2010).
[25] Y. Nakamura and H. Stüben, Proc. Sci., LATTICE2010 (**2010**) 040 [arXiv:1011.0199].
[26] K. Jansen and R. Sommer (ALPHA Collaboration), Nucl. Phys. **B530**, 185 (1998).
[27] M. Göckeler, R. Horsley, A. C. Irving, D. Pleiter, P. E. L. Rakow, G. Schierholz, H. Stüben, and J. M. Zanotti, Phys. Rev. D **73**, 054508 (2006).
[28] V. G. Bornyakov, E.-M. Ilgenfritz, B. V. Martemyanov, V. K. Mitrjushkin, and M. Müller-Preussker, Phys. Rev. D **87**, 114508 (2013).
[29] A. S. Kronfeld, G. Schierholz, and U.-J. Wiese, Nucl. Phys. **B293**, 461 (1987).
[30] F. Brandstater, G. Schierholz and U.-J. Wiese, Phys. Lett. B **272**, 319 (1991).
[31] W. W. Tucker and J. D. Stack, Nucl. Phys. B, Proc. Suppl. **106–107**, 643 (2002).
[32] C. Bonati and M. D'Elia, Nucl. Phys. **B877**, 233 (2013).
[33] G. S. Bali, V. Bornyakov, M. Müller-Preussker, and K. Schilling, Phys. Rev. D **54**, 2863 (1996).
[34] V. Bornyakov, G. Schierholz, and T. Streuer, Nucl. Phys. B, Proc. Suppl. **106–107**, 676 (2002).
[35] V. G. Bornyakov *et al.* (DIK Collaboration), Phys. Rev. D **70**, 074511 (2004).
[36] S. O. Bilson-Thompson, D. B. Leinweber, and A. G. Williams, Ann. Phys. (Amsterdam) **304**, 1 (2003).
[37] In contrast to gradient flow, cooling has no adaptable "flow time step" $\Delta\tau$ and consists of sequential minimizations with respect to single links visited by a sweep through the lattice. In the case of $SU(3)$, this requires a nonanalytical operation called "projection to the group."
[38] M. Lüscher, Commun. Math. Phys. **293**, 899 (2010).
[39] M. Lüscher, J. High Energy Phys. 08 (2010) 071.
[40] M. Lüscher and P. Weisz, J. High Energy Phys. 02 (2011) 051.
[41] M. Garcia Pérez, A. González-Arroyo, J. Snippe, and P. van Baal, Nucl. Phys. **B413**, 535 (1994).
[42] C. Bonati and M. D'Elia, Phys. Rev. D **89**, 105005 (2014).
[43] H. Neuberger, Phys. Lett. B **417**, 141 (1998).
[44] H. Neuberger, Phys. Lett. B **427**, 353 (1998).
[45] P. Hasenfratz, V. Laliena, and F. Niedermayer, Phys. Lett. B **427**, 125 (1998).
[46] H. Neff, N. Eicker, Th. Lippert, J. W. Negele, and K. Schilling, Phys. Rev. D **64**, 114509 (2001).
[47] F. Bruckmann, C. Gattringer, E.-M. Ilgenfritz, M. Müller-Preussker, A. Schäfer, and S. Solbrig, Eur. Phys. J. A **33**, 333 (2007).
[48] Diffusion length given in lattice units a.
[49] E.-M. Ilgenfritz, D. Leinweber, P. Moran, K. Koller, G. Schierholz, and V. Weinberg, Phys. Rev. D **77**, 074502 (2008).
[50] F. Bruckmann, F. Gruber, C. B. Lang, M. Limmer, T. Maurer, A. Schäfer, and S. Solbrig, *Proc. Sci.*, CONFINEMENT8 (2008) 045 [arXiv:0901.2286].
[51] E.-M. Ilgenfritz, B. V. Martemyanov, M. Müller-Preussker, and A. I. Veselov, Phys. Rev. D **71**, 034505 (2005).